Acta Materialia 206 (2021) 116594

Contents lists available at ScienceDirect

Acta Materialia

journal homepage: www.elsevier.com/locate/actamat

Growth of faceted, monolayer-coated nanovoids in aluminium

Xiaofen Tan [a,*], Matthew Weyland [a,b], Yu Chen [b], Timothy Williams [b], Philip N.H. Nakashima [a,*], Laure Bourgeois [a,b,*]

[a] Department of Materials Science and Engineering, Monash University, Victoria, 3800, Australia
[b] Monash Centre for Electron Microscopy, Monash University, Victoria, 3800, Australia

ARTICLE INFO

Article history:
Received 28 July 2020
Revised 17 December 2020
Accepted 18 December 2020
Available online 24 December 2020

Keywords:
Voids
Surfaces
Aluminium alloys
Scanning transmission electron microscopy (STEM)
Crystal growth

ABSTRACT

Voids can cause structural and electrical failure in materials but also show promising properties for use in plasmonics and photonics. Key to understanding the mechanical, optoelectronic and thermal properties of voids is an accurate characterisation of their structure and evolution, in particular of their surfaces. Here we report the formation of voids, coated with a monolayer of tin, in two aluminium alloys. Amongst such voids, those with high aspect ratios ("tubular voids") have been found to grow to hundreds of nanometres in length under certain heat treatment conditions. Using spectroscopy and atomic-resolution imaging in scanning transmission electron microscopy (STEM), we reveal that the voids are covered by a single-atomic-layer tin shell, which is continuous over the entire void surface and has the same atomic structure as the Al matrix. Tubular voids are invariably attached to Sn particles that have a specific orientation relationship with the Al matrix, whilst equiaxed voids are generally not attached to Sn particles exhibiting such an orientation relationship. The aspect ratios of tubular voids show a strong correlation with the coherence between the tin particle and the arrangement of the tin atoms in the void coating, along the growth directions of the tubular voids. These tubular voids could be considered as single-walled nanotubes that are embedded in the aluminium matrix and also as "anti-nanorods". They are of great research interest because they are more likely to cause mechanical or electrical failure than equiaxed voids with the same volume. The coated voids are highly reproducible, controllable and free from contamination, and are therefore ideal for future studies of localized surface plasmon resonances (LSPRs).

1. Introduction

Voids, being essentially large clusters of vacancies, are fundamental defects found in many materials, including metals [1,2] and semiconductors [3]. They can form under a wide variety of conditions, such as thermal quenching [4-6], irradiation (by ions, electrons or neutrons) [7,8], strain [9], creep [10], solidifying particles [11], electromigration [12] and intermetallic oxidation [13]. Voids influence materials properties in different ways. First of all, voids can cause structural and electrical failure in engineering materials, in particular, in some of the most commonly used aluminium alloys [14] and steels [15]. However, voids have also been found to impart strengthening effects on materials, that is, to enhance their yield strength, and the effectiveness was found to depend on the density of voids rather than their size [16]. Void formation *via* electromigration is one of the most critical failure modes in integrated circuits, and is becoming increasingly critical as they scale down [17]. More recently, voids were investigated as sources of confined plasmons, heralding the possibility of their application in photonics or sensing [18]. Nano-scale surfaces created by voids in aluminium were found to be beneficial to significant plasmonic activity [19]. Strongly localized field enhancement was observed in voids embedded in aluminium with localized surface plasmon resonance (LSPR) energies in the extreme UV range [20]. Furthermore, the pristine surfaces in pure Al voids allowed the LSPR properties of pure, oxide-free aluminium nanoparticles to be deduced [20].

Key to how voids form and evolve under different conditions are their surfaces. In pure aluminium, voids can often be annealed out within a short period at moderately elevated temperatures (~180°C) [1]. The annealing behaviour of voids in various metals has been studied, whereby surface energies were determined [21]. Surface energy has recently been found to control the morphological change of shrinking voids (in pure aluminium) during annealing [22]. Segregation of alloying elements to the free surfaces was observed to form coatings on newly formed voids and mature ones, whereby the stability and evolution of voids could be influ-

* Corresponding authors.
E-mail addresses: xiaofen.tan1@monash.edu (X. Tan), philip.nakashima@monash.edu (P.N.H. Nakashima), laure.bourgeois@monash.edu (L. Bourgeois).

https://doi.org/10.1016/j.actamat.2020.116594
1359-6454/

enced, and the properties modified [7,23]. However, there remains little detailed characterisation of void surfaces and morphologies, both in terms of structure and composition. In particular, what drives the development of specific void shapes and the relationship with the void coating is not known.

Here we present observations of coated voids grown in Al(Cu)Sn alloys using different heat treatments. These alloys were chosen because nanovoids were found in association with the solidification of molten tin particles [11]. The AlCuSn alloy is a classic illustration of the potent role played by some microalloying additions, such as Sn, in promoting the precipitation of strengthening phases (the θ' phase in this case) [24-26]. Vacancies have long been known as an essential ingredient in these precipitation mechanisms [27]. In our present work, we show that vacancies can cluster to grow into voids extending to hundreds of nanometres in length in some special cases. These voids have a continuous single atomic-layered tin coating on their surface. Those voids with anomalously high aspect ratios were found to be associated with tin particles having a specific orientation relationship. These can be considered as tubular voids. We propose an explanation for the formation of these tubular voids as well as a general model for the growth of voids. Understanding the growth of high-aspect ratio voids is important as they are more likely to cause electrical or mechanical failure of a material and they might also be considered as anti-nanorods having desirable plasmonic properties.

2. Experimental Methods

The specimens were discs with diameters of ~3 mm and thicknesses of ~0.5 mm, punched from slices of Al-1.7 at. %Cu-0.01 at.-%Sn and Al-0.01 at. %Sn alloys. The heat treatments consisted of 3 fundamental steps, namely solution treatment, followed by an additional heating step, and in most cases, further heating. Each of these steps was followed by quenching into water at 293K (20°C). A schematic diagram of the heat treatments is given in Figure S7a. Solution treatment is a process during which alloying elements dissolve into the matrix and form a solid solution. Quenching then results in a supersaturated solid solution, which will decompose upon heating. The solution treatment was invariably carried out for 30 minutes at 798K (525°C) in nitrate salt baths; the second heating step was mostly at 718K (445°C) for 1 minute in nitrate salt baths, except in one case where it was reduced to 40 seconds to generate a larger number of small tin particles in the liquid state. This second heating step was followed by a cold-water quench, during which nanovoids (as-quenched state) formed due to thermal contraction of the molten Sn particles upon solidification. A third heating step was carried out at 473K (200°C) and 433K (160°C) for a range of times from 10 minutes to 24 hours in oil baths.

The heat-treated specimens were mechanically ground to ~180 μm thickness and then electropolished using a Struers twin-jet Tenupol-5 apparatus with a 33% HNO_3-67% methanol solution at −25°C and 12.5 V, as is conventionally used for aluminium alloys.

Energy dispersive X-ray (EDX) spectroscopy was conducted on a JEOL JEM-2100F TEM operated at 200 kV and equipped with a JEOL EDX Si(Li) detector. The TEM imaging was carried out at 200 kV, with both an FEI Tecnai G2 T20 TEM and an FEI Tecnai G2 F20 TEM with a field-emission gun (FEG), with exception of the TEM images in Figure S11 which were from a JEOL JEM-2100F FEGTEM operated at 200 kV. Atomic resolution HAADF-STEM was performed at 300 kV on a dual aberration-corrected FEI Titan^3 80-300 FEGTEM. A convergence semi-angle of 15 mrad was used, with an inner collection semi-angle of 60 mrad and an outer collection semi-angle of 200 mrad for the HAADF-STEM images.

The HAADF-STEM tilt series were acquired on a dual aberration corrected FEI Titan^3 80-300 FEGTEM operated at 300 kV. All tomography data on this instrument were acquired using FEI Xplore3D, using a convergence semi-angle of 15 mrad and ADF collection semi-angles of 30-200 mrad. The collection inner angle was reduced slightly from the atomic resolution condition above to increase signal, especially at high tilts. The samples were loaded in a Fischione 2020 tomography holder allowing a tilt range of ±72°, limited only by sample thickness. Tilt series were acquired with a 2° tilt increment. Tomographic alignment and reconstruction were carried out using code developed [28] in IDL (Harris Geospatial, USA). Reconstruction was carried out iteratively using SIRT [29] with 30 iterations. Segmentation of the volumes was carried out manually using Amira 6 (Thermo Fischer Scientific, USA), and visualization was *via* surface render of selected segmented volumes. For Figure S14 the tilt series was acquired manually on the FEI Tecnai G2 F20 FEGTEM, the tilt range was −60° to 62°, with a tilt step of 10° (from 0° to ±60°) or 2° (from 60° to 62°).

The atomic models were generated using CrystalMaker [30].

3. Results

3.1. Growth of voids under various heat treatments

Both Al-1.7 at. %Cu-0.01 at. %Sn and Al-0.01 at. %Sn alloys subjected to similar heat treatments were investigated. Voids in AlCuSn were found to be highly reproducible in their yield (number of voids per unit volume), sizes and morphologies under a given heat treatment condition; they also exhibited more diversity, as the heat treatments changed, and more intriguing features than the voids found in AlSn.

Fig. 1(a) gives typical examples of voids in AlCuSn in the as-quenched state and after a range of subsequent heat treatments. The as-quenched condition refers to when nanovoids form due to thermal contraction of the Sn particles as they solidify from the molten state [11]. This is why each void is attached to a single tin particle; these tin particles are the β-Sn phase [11]. Following further heating at moderate temperatures (160°C or 200°C), much larger voids were observed, indicating significant void growth.

As can be seen in Fig. 1 and Figure S1, the voids exhibit different morphologies. Voids with aspect ratios less than 1.6 were all categorized as equiaxed voids. This limit was determined from the distribution of void aspect ratios associated with larger tin particles, i.e. those with widths greater than 70 nm where the void aspect ratio distribution is very uniform (Fig. 1(b) – see the region shaded blue). The mean of this aspect ratio distribution is 1.2 with a standard deviation of 0.2. All voids within 2 standard deviations of this mean aspect ratio (the standard 95% confidence interval) have been designated as equiaxed, giving the definition of equiaxed an aspect ratio upper bound of 1.6. This definition takes in all small equiaxed voids, large equiaxed voids and mature voids.

Mature voids, larger than 100 nm in the shortest dimension and less faceted than the other three types of voids, are present in the specimens that were heated for 30 minutes or longer at 200°C and 2 hours or longer at 160°C (see for example, the voids labelled “18 h @ 200°C” and “18 h @ 160°C” in Fig. 1a). Large equiaxed voids are generally smaller than mature voids and are surrounded by precipitate-free zones (see Figure S1 in the supplementary materials). Small equiaxed voids, in contrast, are not surrounded by precipitate-free zones.

Voids with aspect ratios greater than 2 have been classified as tubular (green shading in the graph of Fig. 1(b)). This designation is essentially qualitative and arbitrary and leaves a number of voids in between the equiaxed and tubular categories and we assign these to an intermediate class of voids having medium aspect ratios (shaded in yellow in the graph of Fig. 1(b)).

Tubular voids are invariably associated with smaller Sn particles (i.e. those with diameters of about 20 nm to 40 nm), as high-

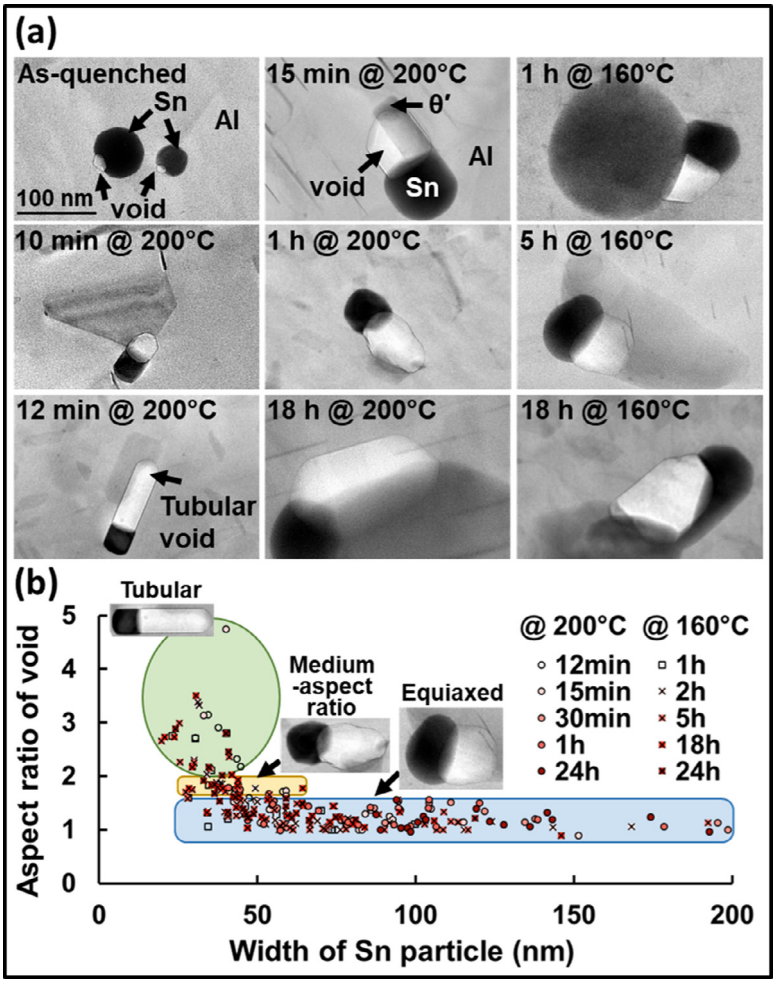

Fig. 1. A summary of void sizes and shapes after different heat treatments. (a) Bright field transmission electron microscopy (TEM) images of typical voids in Al-1.7 at. %Cu-0.01 at. %Sn, in the as-quenched state and after a range of subsequent heat treatments (given on top of each image). All images are at the same scale indicated at top left. An added heating step at a lower temperature led to significant growth of the voids. (b) A plot showing the aspect ratio of voids as a function of the width of the attached tin particle. Most of the tin particles with widths greater than 70 nm are attached to voids with aspect ratios within 2 standard deviations of the mean of 1.2. Given that the standard deviation in these aspect ratios was determined to be 0.2, all voids with aspect ratios less than 1.6 were categorized as equiaxed voids (blue shading). Among the voids attached to small tin particles, some voids (around 10% out of the total number of voids) possess high aspect ratios ($>$ 2) and they can thus be considered as tubular voids (green shading). This leaves voids with aspect ratios between 1.6 and 2 and we classify these as having medium aspect ratios (yellow shading).

lighted in Fig. 1(b). Despite the general presence of tubular voids after most heat treatments, their proportion is the highest (50%) after one particular added heating step, namely 12 min at 200°C (Figure S2 in the supplementary materials). Note that the heating conditions here and onwards refer to after the as-quenched state, unless stated otherwise.

Whereas the void yield in AlCuSn is very high and highly reproducible across samples, in AlSn it is variable from sample to sample, even under the same heat treatment conditions. Even in the samples with the most voids per unit volume, the yield is poorer than in AlCuSn by a factor of 3. In addition, after a heating time of longer than 1 hour, no voids were observed in AlSn. This implies that voids are generally not as stable in AlSn as compared to AlCuSn.

3.2. Continuous single-atomic-layer tin shell isostructural with the Al matrix

Typically, voids from AlSn and AlCuSn are each attached to a tin particle (*e.g.*, Figure S3). Additionally, for AlCuSn, there is also a Cu-containing precipitate (the θ' phase (Al_2Cu)) located at the void shell, either attached to the Sn particle or separated from it. As shown in Fig. 2, Figure S3 and the movies in the supplementary materials (Movie 1 and Movie 2), the shell has single-atomic-layer thickness, is continuous, is composed of tin and is isostructural with the Al matrix.

To be specific, imaging by HAADF-STEM shows that the segregated atoms on the shell have a higher projected atomic number (Z) than Al. In addition, in the case of both AlSn and AlCuSn, energy dispersive X-ray spectroscopy (EDX) (Figure S3c, d and e) and electron energy loss spectroscopy (EELS) (Figure S3f and g) demonstrate that the shell consists of Sn atoms without any detectable Cu in the case of AlCuSn.

When viewed edge-on, the shell displays the same projected structure as the Al matrix, both along the [001] zone (Fig. 2c) and the [011] zone (Fig. 2d) of the matrix. This strongly suggests that the Sn atoms in the shell have the same structure as the Al matrix, meaning that they have taken on a different atomic arrangement to that in the associated β-Sn particle (which has a tetragonal crystal structure). This also means that, no surface reconstruction across the matrix / coating / void interface was observed, relative to the supporting Al matrix.

Annular dark-field STEM tomography (Fig. 2e, f and g) revealed the coating to be continuous all around the void surface, not just

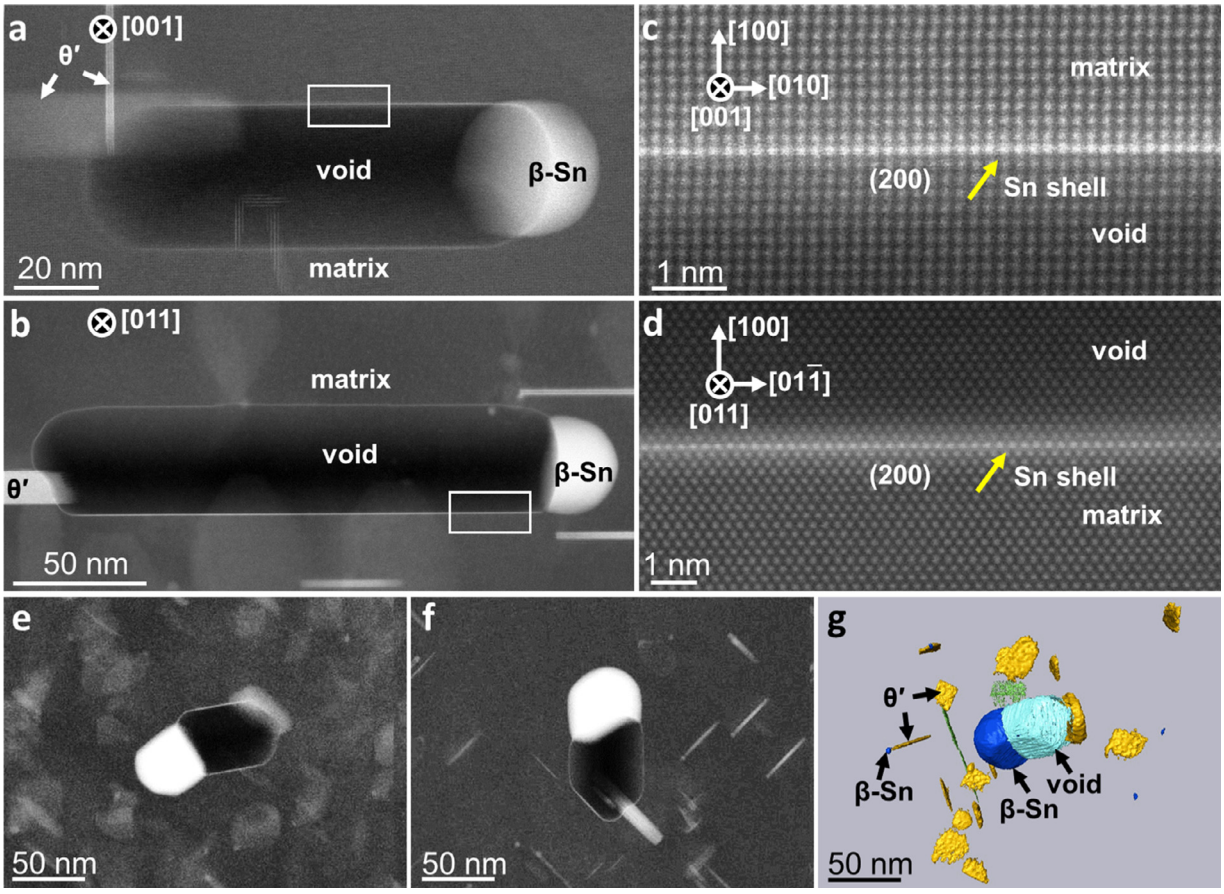

Fig. 2. Structural analysis of the void shells. (a, b) High-angle annular dark field scanning transmission electron microscopy (HAADF-STEM) images of two tubular voids in AlCuSn. One is viewed along [001] (a) and the other along [011] (b). The atomic resolution images, c and d, of the regions in the white rectangles in a and b respectively are also shown. The yellow arrows point to the Sn shells. The contrast in c and d suggests that the Sn shells are single atomic-layered and continuous along the (200) facets. The specimens containing these two voids were subjected to heating for 12 minutes (a) and 15 minutes (b) at 200°C. (e, f) Images from tilt series taken from two different void / particle systems, with the tilt axes perpendicular and orthogonal to the void long axes respectively (Movie 1 and Movie 2 respectively in the supplementary materials). These results are indicative that the Sn shell is continuous over the entire void surface. The third heating step was 1 hour at 160°C. (g) Surface render of a hand-segmented tomographic reconstruction of the void and surroundings shown in (e). In this figure, the blue represents Sn particles, the cyan is the void, and the golden and green features represent θ' and θ'' precipitates respectively. A movie of this visualization is available in the supplementary materials (Movie 3). Note the absent cyan void coating in Movie 3 is due to the classical 'missing wedge' problem [28] due to limited maximum tilt.

on the facets shown in Fig. 2a–d. Results of the tomographic visualization, Movie 3 in the supplementary materials, indicate this. Note that the absence of the coating in the reconstruction in this movie on the top and bottom of the void (the 'missing' cyan) is a consequence of the classical 'missing wedge' problem [28] due to limited maximum tilt.

3.3. Orientation relationships between the tin particle attached to a tubular void and the matrix

The great majority of voids were observed to have nearly the same width as the attached tin particles (see Figure S4), except in the as-quenched state, when voids have just formed. In addition, after the third heating step of 12 min at 200°C, there is an inverse relationship between the aspect ratios of voids and the widths of the attached tin particles. These results indicate that the growth of voids begins with their widening to match the width of their parent tin particle. As mentioned above, tubular voids were invariably found attached to the smaller tin particles, *i.e.* those with diameters of about 20 nm to 40 nm. Furthermore, all of these tin particles were found to share a specific orientation relationship (OR) with the matrix, namely $[110]_{Al} \parallel [100]_{Sn}$ and $(001)_{Al} \parallel (001)_{Sn}$ (OR1, see Figs. 3 and 4a). Tin particles attached to medium-aspect ratio voids mostly have widths of about 30 nm to 60 nm, some satisfying OR1 with respect to the matrix. A single case of a medium-aspect ratio void exhibiting a different OR was also observed, namely $[110]_{Al} \parallel [010]_{Sn}$ and $(001)_{Al} \parallel (100)_{Sn}$ (OR2, see Fig. 4a and Figure S5 in the supplementary materials). In contrast, Sn particles attached to equiaxed voids generally showed entirely different orientational relationships such as $[001]_{Al} \parallel [1\bar{1}1]_{Sn}$ and $(020)_{Al} \parallel (21\bar{1})_{Sn}$ (OR3, see Fig. 4a and Figure S6).

To distinguish whether the orientation relationship or the tin particle size is the determining factor in forming a tubular void, we attempted to generate a greater number of small tin particles by making only a small modification to the heat treatment with which we had obtained the largest yield of tubular voids so far. Referring to the general heat treatment regime applied to our alloys in Figure S7(a), we changed the intermediate heating step to be only 40 seconds in duration (instead of 1 minute) at 445°C followed by a cold-water quench. Otherwise, the subsequent heating for 12 minutes at 200°C remained unchanged. As shown in Figure S7b in the supplementary materials, this led to a larger number of small tin particles attached to voids (~40 nm wide). However, the proportion of tubular voids was still around 50% of the total number of voids, which is similar to that of the original heat treatments. At the same time, more small tin particles were attached to equiaxed voids compared to the original heat treatments. Therefore, one can conclude that orientation relationship is a critical fac-

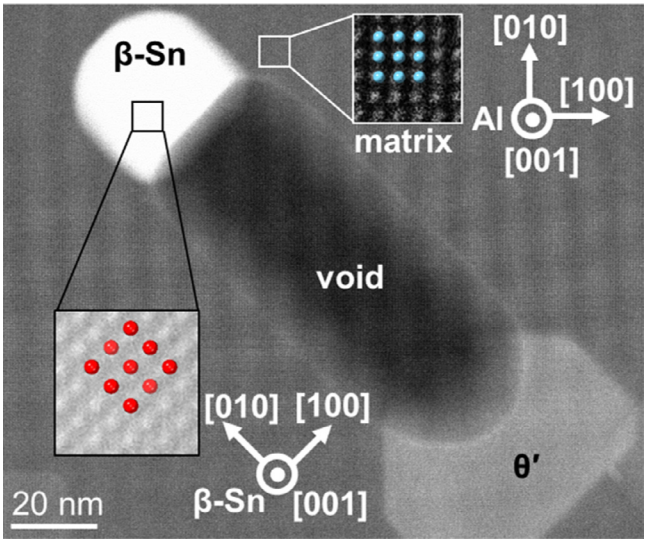

Fig. 3. A HAADF-STEM image of a tubular void in AlCuSn viewed along [001] of the matrix. The third heating step was 12 min @ 200°C. The insets are the corresponding atomic-resolution images for the matrix (white frame) and β-Sn (black frame). The orientation relationship between the matrix and the Sn particle is $[110]_{Al}$ || $[100]_{Sn}$ and $(001)_{Al}$ || $(001)_{Sn}$ which we defined as OR1 (see also Fig. 4a). The coloured dots show the projection of a single face-centred cubic unit cell of Al (blue) and a single tetragonal cell of β-Sn (red). The ~10 nm wide lattice contrast is a moiré pattern between the fixed lattice of the Al and the fixed lattice of the scanned pixels.

tor, in addition to the tin particle being small, for the development of tubular voids.

We have found that the majority of tubular voids grow along $<110>_{Al}$ and a minority grow along $<100>_{Al}$ (Fig. 4a). In both cases, the fact that $a_{\beta-Sn} = b_{\beta-Sn} = 5.83$ Å $\approx \sqrt{2}a_{Al} = 5.72$ Å results in coherence between the tin particle and the matrix along $<110>_{Al}$ and $<100>_{Al}$. These directions are precisely the same as the long axes of the tubular voids. Detailed illustrations of a typical tubular void are given in Fig. 4b-e (more schematics are available in the supplementary materials, see for example Figure S8 and Figure S9). In addition, the cross-sectional structure of the tubular void illustrated in the schematics was determined from high angle tilt series, as detailed in the supplementary materials (see "Geometry of the tubular void (from AlCuSn) shown in Fig. 3").

We characterised the degree of coherence between the tin particle and the surrounding matrix through the size of the coincident site lattice (CSL) [31], as described in the supplementary materials (see "CSL analysis"). Using this method, we found that the degree of coherence increases as the aspect ratio of the voids increases (see Fig. 5). In addition, we infer that the degree of coherence between the tin particle and the tin shell increases as the aspect ratio of the void increases, because HAADF-STEM observations indicate that the structure of the tin shell is the same as that of the matrix.

4. Discussion

We reported the formation of nanovoids with single-atomic-layer Sn coatings in two aluminium alloys. The nanovoids in AlCuSn investigated in this work were observed to mostly (about 96%) have mean dimensions of 40 nm to 200 nm after a third heating step of 1 hour at 160°C, or 10 minutes at 200°C (see Fig. 1b). The mean dimensions were obtained by averaging the measured widths and lengths, given that a significant fraction of these nanovoids had a tubular shape. In contrast, in pure aluminium, the largest voids observed typically have mean dimensions of approximately 20 nm [1]. Such voids form during quenching from high temperatures (over 500°C) when the equilibrium vacancy concentration is higher [32]. They are uncoated by solute atoms and shrink during heating at 100°C or even under electron beam irradiation at room temperature [22]. However, the coated voids reported here, which were generated by thermal contraction of tin particles [11], remained unaffected by the electron beam, at least at room temperature. In addition, the current research reveals growth of such coated voids during subsequent heating at 160°C and 200°C in the absence of the electron beam, in bulk specimens. A possible reason for the greater stability of voids in AlCuSn compared with voids in pure Al is the presence of the Sn monolayer at the void surface.

The significant growth of coated voids may be explained by the presence of quenched-in vacancies initially trapped by Sn solute and released at temperatures of 160°C and 200°C [33,34]. The ability of Sn atoms to trap vacancies is well known [27]; more recently [33,34], Sn has been shown to not only trap vacancies but also release them on demand. We propose that this scenario may be at play here, based on the following evidence. Significant solute Sn in the as-quenched state is suggested by the high number density of θ' precipitates in the specimen after subsequent heating of merely 15 minutes at 200°C. This is because the θ' phase nucleates with great difficulty without the aid of Sn [35]. The existence of a significant amount of solute Sn was confirmed through the measured sizes and number densities of tin particles, whether attached to voids or not, in the as-quenched state. This is detailed in the supplementary materials, see "Estimation of Sn solute concentration in the as-quenched state" and "Estimation of Sn quantity attached to the θ' platelets under a subsequent heating condition of 20 minutes at 200°C". In addition, the diffusion coefficients of solute Sn were estimated to be lower than monovacancies in Al [36], ensuring a sufficient concentration of vacancies remains in the alloy. This is detailed in the supplementary materials, see "Estimation of the diffusivity of solute Sn and vacancies during subsequent heating". Void growth (as measured by the projected widths and lengths) after 15 minutes at 200°C is comparable to that for 1 hour at 160°C. The generally faster kinetics at 200°C than 160°C suggests that more vacancies were released at 200°C [37,38].

The voids in AlCuSn are polyhedra bounded by perfectly flat {200} and {111} facets. These void facets have also been found in other face-centred cubic metals such as pure aluminium [22], copper, silver and gold [6] as well as hexagonal close-packed crystals including titanium [39] zirconium [40] and magnesium [41]. In the present work, we show that, in AlCuSn and under certain heat treatments, some of these facets grow at the expense of others to form tubular-shaped nanovoids. In the following we propose a model for the growth of the different void morphologies observed.

4.1. Growth model proposed for coated voids in AlCuSn

In AlCuSn, the majority of voids are equiaxed. This could be reasonably explained by an equiaxed shape having a smaller surface area than an elongated one with the same volume, thus having a lower surface energy. In the early stages of growth, voids mostly have widths that are approximately equal to those of the attached tin particles, regardless of the aspect ratios of the voids. This observation, firstly, indicates that the widths of the tin particles limit the widths of the attached voids (particularly tubular voids). Secondly, it suggests that broadening has priority over elongating in the early stages of void growth, *i.e.* until the void has reached the same width as the attached tin particle, which is confirmed by the existence of voids in their early stages of evolution with aspect ratios that are less than one. This is consistent with the fact that broadening across the tin particle does not increase the surface energy of the whole particle-void-matrix system as much as elongating into the matrix, given the same increase in void volume (see Figure S10 in the supplementary materials).

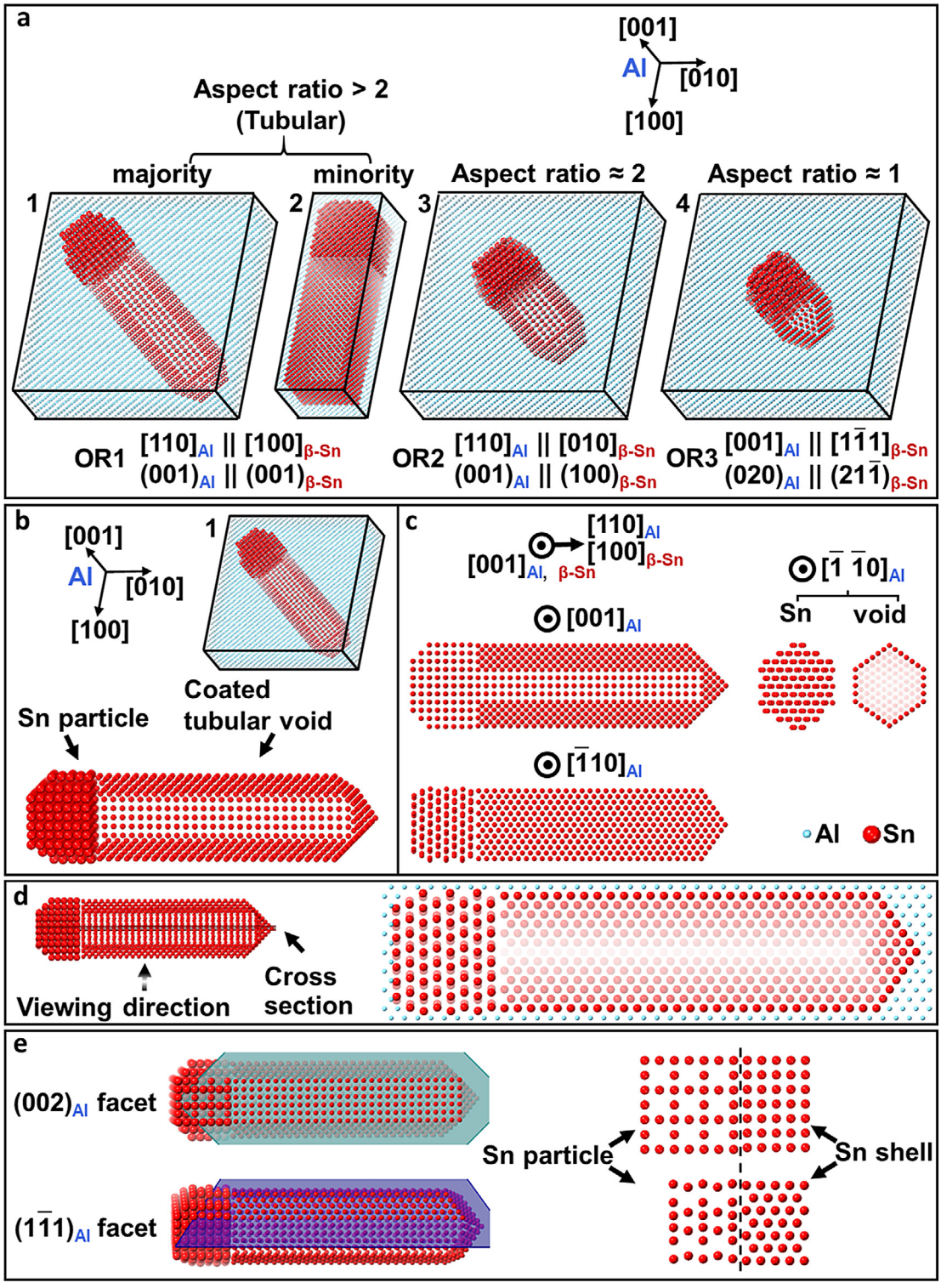

Fig. 4. Atomic models describing all types of voids encountered in the present study. (a) Atomic models illustrating the four main void types in AlCuSn corresponding to different aspect ratios. Type 1 is the most common tubular void: the void grows along $<110>_{Al}$ ($[110]_{Al}$ in this particular example) and the orientation of the tin particle satisfies OR1. Type 2 is a less common tubular void: the orientation of the tin particle satisfies OR1 and the void grows along $<100>_{Al}$ ($[100]_{Al}$ in this particular example). Type 3 is neither a tubular void nor an equiaxed void: the void grows along $<110>_{Al}$ ($[110]_{Al}$ in this particular example) and the orientation of the tin particle with respect to the matrix is classed as OR2. Type 4 is an equiaxed void where the orientation of the tin particle with respect to the matrix satisfies OR3. (b) A schematic 3D view showing a type 1 tubular void. (c) Views of the type 1 tubular void system from various crystallographic directions. The geometry of the cross-section perpendicular to the long axis of the tubular void was determined from high-angle tilt series (detailed in the supplementary materials, see "Geometry of the tubular void (from AlCuSn) shown in Fig. 3"). For simplicity, the minor facets are not shown. (d) A type 1 tubular void cross-sectioned perpendicular to and projected along $[\bar{1}10]_{Al}$. Here the facets and lattice structure were determined from the contrast in the atomic resolution HAADF-STEM images. (e) To show the coherence between the tin particle and the void shell, the main facets of the void shell were extracted together with the adjacent tin particle structure and positioned parallel to the plane of the page with the void growth direction being horizontal. These facets are $\{002\}_{Al}$ and $\{111\}_{Al}$ and are shown on the particles as the shaded blue / purple areas, respectively. The dashed line represents the tin particle / void interface.

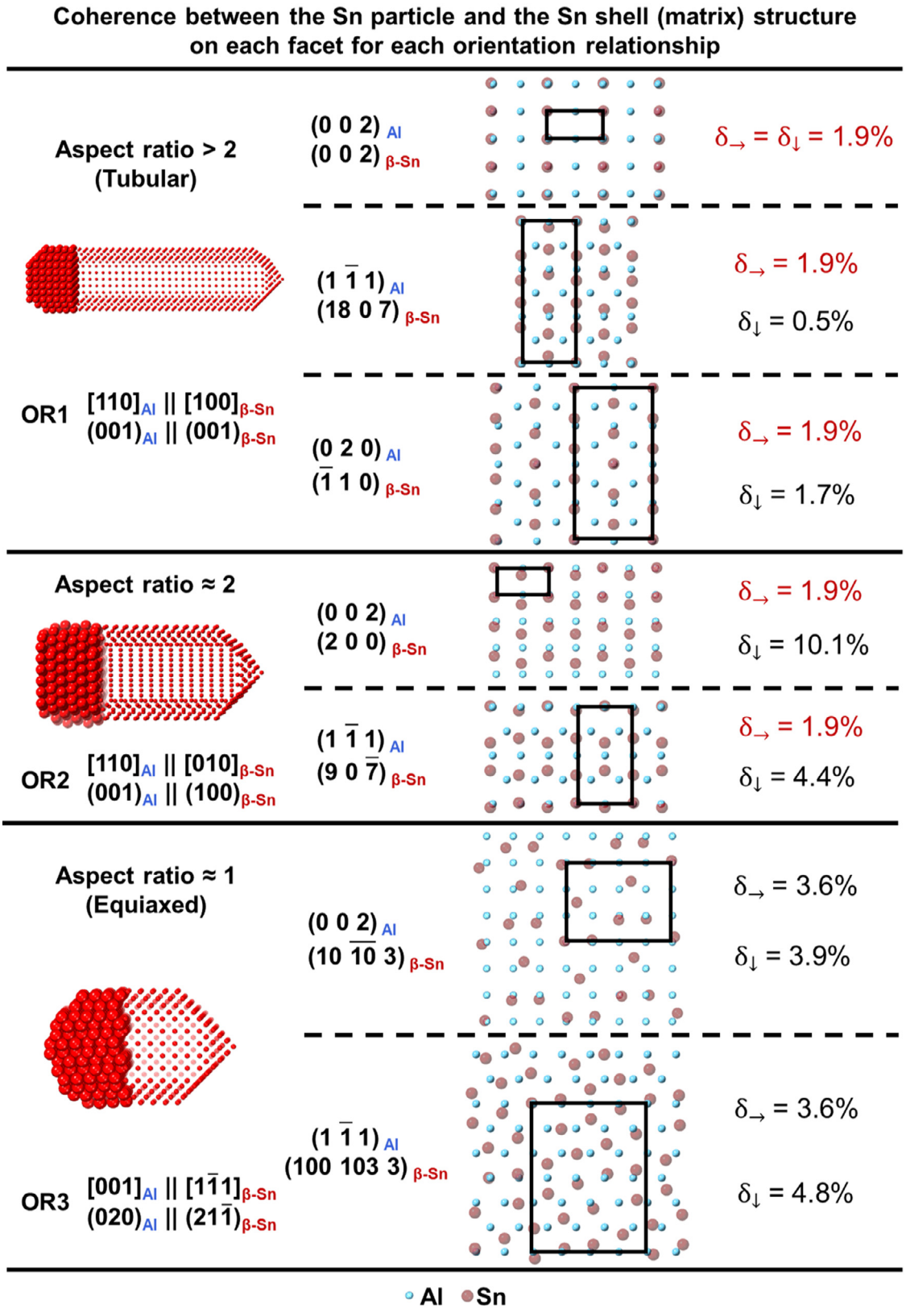

Fig. 5. Quantification of the degree of coherence by the coincident site lattice (CSL) method [31]. The degree of coherence between the tin particle and the surrounding matrix (in AlCuSn) was characterised using the coincident site lattice (CSL) method for the 3 orientation relationships corresponding to different aspect ratios given in Fig. 4. The black frames represent the unit cells of the CSLs. The mismatch, δ, in each CSL was calculated along each direction (shown by arrows, the red texts highlighting the directions of coherence). An overall decreasing trend in the coherence can be seen in this figure as the aspect ratio of the void decreases. Since the tin shell has the same atomic structure as the matrix, we infer a decreasing trend in the coherence between the tin particle and the tin shell as the aspect ratio of the void decreases.

After the first stage of growth where a void reaches the same width as its supporting tin particle (as discussed above), the subsequent elongation of a void into the matrix, away from the tin particle / void interface, results in the same amount of increase in surface energy as would further expansion beyond the width of the attached tin particle coplanar to the void / particle interface (scenario 1 in Figure S10). Therefore, we expect voids to develop equiaxed shapes. While this is true for the majority of voids in AlCuSn over all heat treatment regimes, under certain conditions, a substantial fraction of voids grew into unusual tubular shapes (see Fig. 1, Figure S2 and Figure S7).

Tubular voids were observed to have widths about the same as the attached tin particles, similarly to the "sausage voids" reported over 50 years ago [21]. Such morphologies strongly suggest that, in their formation, elongation had priority over expansion beyond the width of the attached tin particle. Given that the elongated morphologies of tubular voids do not minimize surface energy, what are the reasons for their formation? Since voids are also a type of precipitate that results from the clustering of vacancies, the strong correlation observed between the aspect ratio of the voids and the crystallographic orientation of the attached Sn particle reminds us of precipitates having large surfaces where there is coherence with the matrix. Therefore, the key to understanding the formation of tubular voids might be the distribution of Sn atoms within the monolayer shell. Our atomic-resolution imaging revealed that the tin shell has the same structure and orientation as the Al matrix. This observation is consistent with elastic energy analyses and first-principles calculations showing that the segregation of solute Sn atoms onto the void / matrix interfaces is favoured [42,43]. Based on this observation, we propose a mechanism for the development of tubular voids, which is detailed below.

In the present work, Sn particles attached to tubular voids were determined to exhibit a particular orientation relationship with the Al matrix, which we described and called OR1 (see Fig. 3 and Fig. 4a). The majority of tubular voids grow along the $<110>_{Al}$ direction and a minority along $<100>_{Al}$. In both cases, the crystal structure of the Sn particle matches well with the matrix and therefore also tin shell on the main facets, *i.e.* $\{1\bar{1}1\}$ and {002} facets for $<110>_{Al}$ oriented tubular voids and {200} facets for $<100>_{Al}$ oriented ones. We infer that the coherence between the tin particle and the matrix (and therefore also the tin shell) could be advantageous to the development of a tubular void and the reason has two components to it. On one level, the good match between the particle and the matrix may hinder the segregation of solute Sn atoms onto the tin particle due to the lack of accommodating sites for the solute, thus hampering growth of the tin particle. As a result, the small tin particle size would limit the width of the void. This is consistent with our observation of a one-to-one correspondence between the measured widths of the particle and the void at their common interface (see Figure S4). Similar mechanisms have also been reported in the formation of nanowhiskers [44,45]. On the other hand, the coherence between the tin particle and the tin shell could facilitate the elongation of tubular voids.

For the growth of a void, a plausible mechanism is that vacancies come into the void *via* its tip (Fig. 6a). This is supported by the general observation that the tip of a tubular void is rounded rather than faceted (Fig. 2b and Figure S11) and therefore consists of many atomic steps, making it easier for vacancies to penetrate through the discontinuities than the facets. In other words, there is a direct link between the round shaped tip of a tubular void and void elongation. As vacancies come in, the void grows and so does its coating. We can envisage two sources of tin atoms for the growth of the tin shell. Firstly, the coating could be supplied by solute Sn atoms in the vicinity of the void: the void / matrix interfaces act similarly to grain boundaries and free surfaces in favouring the segregation of alloying elements [42], and the segregation of Sn has been calculated to lower the surface energy of Al [43]. A second possibility is that the coating could be supplied by the attached tin particle (Fig. 6a). In the case of OR1 (and to a lesser extent OR2) where there is coherence between the tin particle and the Sn coating along the long axis of a tubular void, not only should the strain at their interface be reduced, but smaller atomic shifts would be required for the Sn atoms from the particle to coat the void across the void shell / tin particle interface. Therefore, the energy barrier [35,41] for the elongation of such a void could be expected to be lower compared to expansion of the void beyond the width of the attached tin particle, the latter case possibly requiring nucleation of new steps, which might be associated with a high energy barrier. This suggests that anisotropic shapes like tubular voids could form more easily under fast kinetic conditions [46], such as in the early stages of growth. This would account for the prevalence of tubular voids in samples heated only for a short time (12 min @ 200°C) despite the fact that tubular morphologies have higher surface areas and, consequently, higher total surface energies compared to equiaxed shapes with the same volume. Under conditions of prolonged heating, no tubular voids were observed and the widths of some mature voids exceed those of their attached tin particles by up to 50% (see for example, the void labelled "18 h @ 200°C" in Fig. 1a). These results strongly suggest that, in the late stages of growth, tubular voids could change shape in order to reach the equilibrium shape according to the Wulff construction [47,48]. The above proposal, however, needs to be validated using *in-situ* heating.

So far, OR1 seems to account for the development of tubular voids in AlCuSn and the absence of tubular voids in AlSn could also be explained by the absence of this orientation relationship in that system [49]. Orientation relationship 1 seems to also be responsible for the tin particle being small and tubular voids being narrow, as explained above.

If what is discussed above could account for the correlation between OR1 and tubular voids, we should be able to understand other aspect ratios similarly. The three orientation relationships are illustrated in Fig. 6b, where the degree of coherence between the tin particle and Al can be seen to have the relationship: OR1 > OR2 > OR3. Orientation relationship 2 (OR2), which is $[110]_{Al}$ || $[010]_{Sn}$ and $(001)_{Al}$ || $(100)_{Sn}$, is a different orientation relationship to OR1 since $(100)_{Sn}$ is not equivalent to $(001)_{Sn}$. However, in OR2, $[010]_{Sn}$ being parallel to $[110]_{Al}$ also provides some degree of coherence between the tin particle and the void shell and matrix (see Figure S9). The lowest coherence between the tin particle and Al, however, is in OR3, corresponding to large equiaxed voids, the antithesis of tubular voids in that the tin particles can grow significantly (and consequently, the voids could also broaden noticeably). The observation of precipitate-free zones around large equiaxed voids supports the view that the large tin particles (and large equiaxed voids) grew by draining local solute Sn atoms and vacancies in the nearby matrix. It is worth mentioning that the volume of a typical large equiaxed void is about 4 times that of a typical tubular void and about 10 times that of a small equiaxed void, and that the volume of a tin particle attached to a large equiaxed void is about 10 times that of a tin particle attached to a small equiaxed void. Again, we assume that the depths of the voids and tin particles equal their respective projected widths. Therefore, we consider that as a result of the growth of tin particles, the number of solute Sn atoms removed from the matrix surrounding a large equiaxed void could be several times that around a small equiaxed void. In addition, the volume of an as-quenched void is negligible compared to that of a grown void observed in this work (see Fig. 1a). Based on the arguments above, during the growth of voids, the total volume of vacancies depleted from the matrix around a large equiaxed void is also several times that around a tubular void or a small equiaxed void. The substantial depletion of both solute Sn

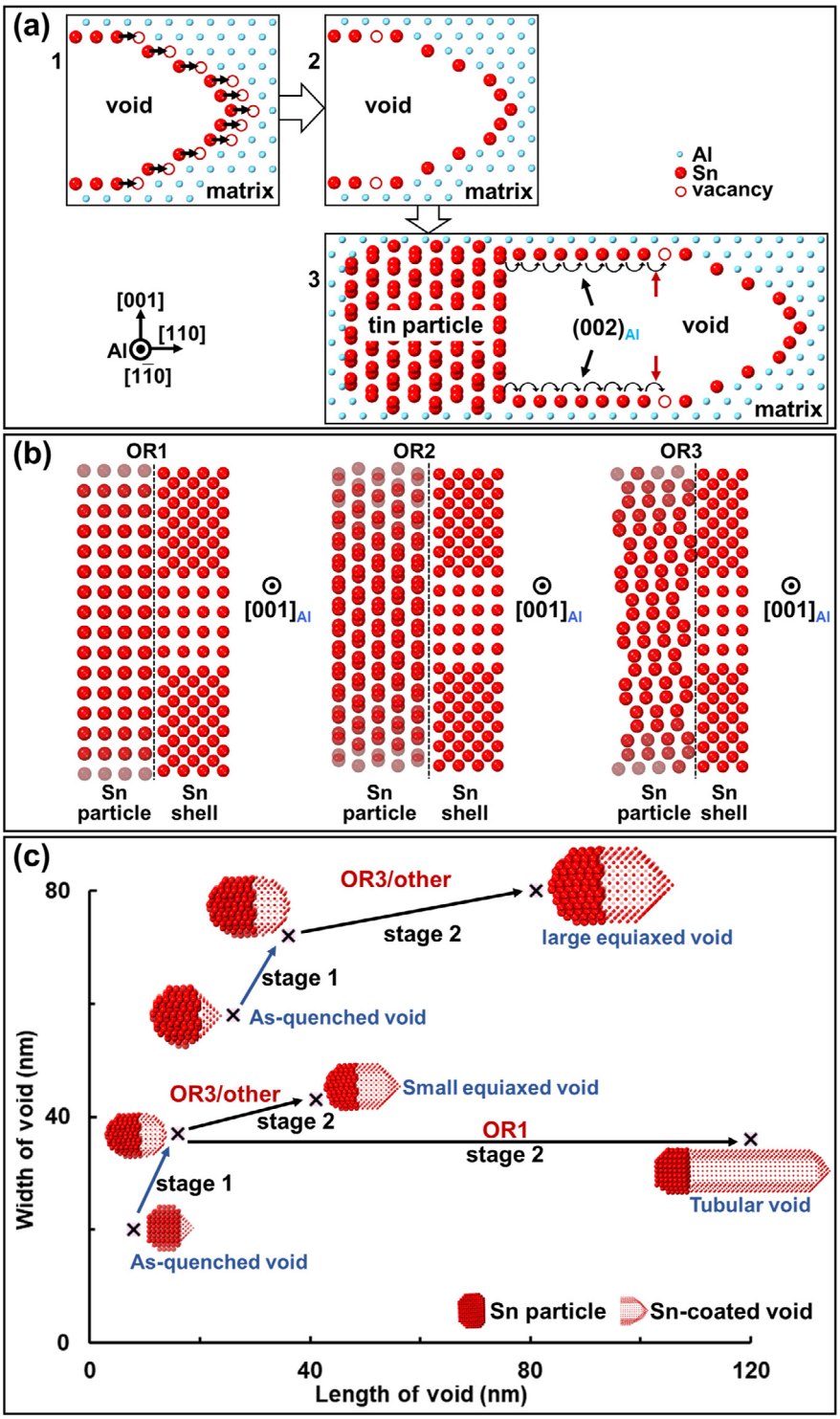

Fig. 6. A diagrammatic proposal for the evolutionary pathways of voids in AlCuSn. (a) A schematic diagram illustrating the proposed growth mechanism of the tubular voids, showing only a cross-sectional slice. For clarity, only the tip of the void is shown in 1 and 2. For each Sn-vacancy pair connected by a black arrow in 1, the Sn atom and vacancy exchange locations. The total effect is the void lengthening by one atomic layer while a vacancy is created on each $(002)_{Al}$ facet of the Sn shell (shown in 2). For simplicity, vacancies inside the void were not drawn. Note that from 1 to 2, the total number of Sn atoms in the shell remained unchanged. The growth of the Sn shell, facilitated by the attached tin particle that exhibits OR1 with the matrix, is illustrated in 3. Starting from the regions marked by the red arrows, the neighbouring Sn atoms in the Sn shell come to fill the vacancies, causing a sequential movement of vacancies toward the tin particle and eventually pulling Sn atoms from the tin particle itself. (b) Schematic diagrams of the three orientation relationships between the tin particle and the Sn shell. The black dotted lines represent the interfaces between the Sn particles and the Sn shells which were revealed to have the same structure as the matrix. The degree of coherence between the Sn particle and the Sn shell has the relationship: OR1 > OR2 > OR3. (c) A schematic diagram summarizing the proposed growth stages of voids according to observations from different heating times at 200°C. The lower part of the diagram illustrates the development of small equiaxed and tubular voids, and the upper part shows that the large voids in their as-quenched states [11], attached to large tin particles, grow into large equiaxed voids. Stage 1 is predominantly broadening, the aspect ratio of the void at the end point being less than 1. Stage 2 is mainly lengthening (leading to tubular voids) or lengthening accompanied by broadening (leading to equiaxed voids). Note that this diagram does not show the late growth stages where all voids become mature voids (*i.e.* larger than 100 nm in the shortest dimension, less faceted than the other types of voids and equiaxed).

and vacancies is highly likely to be responsible for the formation of the precipitate-free zones observed around large equiaxed voids, because solute Sn promotes the nucleation of θ' precipitates [25], and vacancies also play an important role in precipitation [50].

In summary, the following stages of void growth are proposed (see Fig. 6c):

Stage 1. Broadening and a lesser extent of lengthening resulting in a void with aspect ratio less than 1 and a width that is about the same as the attached tin particle.

Stage 2. Lengthening into a tubular void or medium-aspect ratio void (for voids attached to tin particles that exhibit OR1 or OR2 with the matrix) or lengthening accompanied by broadening to result in an equiaxed void (for voids attached to tin particles that satisfy OR3 with the matrix). Further experimental evidence is available in the supplementary materials, see Figure S12.

Throughout the heating process, the attached tin particle might also grow or change shape. Afterwards, with longer heating, all voids continue to grow and eventually become mature voids, which are generally larger than 100 nm in the shortest dimension and less faceted than the other types of voids preceding maturity.

Tubular voids are more likely to cause electrical or mechanical failure of a material, compared to equiaxed voids with the same volume. Our findings may suggest ways of preventing the unwanted growth of tubular voids. Conversely, tubular void growth may be desirable, such as for the design of new nanomaterials. For example, the tubular voids investigated in this study may be regarded as empty [22] monolayer tin nanotubes. However they differ from the conventional notion of nanotubes [51] because they cannot exist as free-standing entities in the absence of the supporting matrix in which they are embedded. Furthermore, the single-atomic-layer tin shell exhibits a similar structure to aluminium in projection when viewed edge-on. Therefore, a distinctive electronic structure is expected and further studies to prove this would be worthwhile. In addition, the presence of the tin shell is highly likely to result in different plasmonic properties compared to uncoated voids in pure aluminium [20]. Future localized surface plasmon resonances studies of this void system are feasible because the sizes and shapes of the coated voids are highly reproducible when a certain heat treatment is performed. The sizes and morphologies of these voids can also be changed easily by varying the heat treatment, as has been explored in detail in the current work. Last but not least, this system is pristine and free of oxides and other contaminants. A shortened void forming step could be helpful to narrow the size range of the as-quenched voids and also that of the grown voids following subsequent heating. To selectively generate tubular voids or equiaxed voids, size control might not be sufficient. We might also need to control the orientation relationship of the particles associated with voids. The main limitation of our current experimental setup is the lack of excess vacancies to grow the voids. This must be addressed if one is to farm tubular voids for device applications. One way to boost the excess vacancy concentration might be to use vacancy trapping elements other than Sn.

5. Conclusions

Coated voids in an Al-1.7 at. %Cu-0.01 at. %Sn alloy were observed to grow to hundreds of nanometres in length with very high aspect ratios, giving them tubular shapes. This special type of tubular voids is invariably attached to Sn particles having a specific orientation relationship with the Al matrix of $[110]_{Al} \parallel [100]_{Sn}$ and $(001)_{Al} \parallel (001)_{Sn}$. Compared to voids in pure aluminium, whose major axes are oriented along $<001>_{Al}$, the major axes of tubular voids in AlCuSn are almost always oriented along $<110>_{Al}$ with occasional exceptions where the orientations are along $<001>_{Al}$. What is most notable, however, is that the orientation relationship between the Sn particles and Al matrix is the same in all cases of tubular void formation, regardless of their axial orientations. All voids were found to be coated with a continuous, single atomic layer of tin with the same structure as that of the surrounding aluminium matrix. Based on this knowledge, we proposed a growth mechanism whereby the Sn particle / Al matrix orientation relationship facilitates tubular void growth due to the coherence between the Sn shell and its attached particle.

Declaration of Competing Interest

The authors declare that they have no known competing financial interests or personal relationships that could have appeared to influence the work reported in this paper.

Acknowledgements

The authors acknowledge the instruments and scientific and technical assistance at the Monash Centre for Electron Microscopy, Monash University, the Victorian Node of Microscopy Australia. XT is grateful for a Monash Graduate Scholarship, a Monash International Postgraduate Research Scholarship and an Alexander Moodie Scholarship. XT is indebted to Mr. Renji Pan, Dr. Russell King and Dr. Peter Miller for training and technical assistance. Thanks also extend to Dr. Yong Zhang, Dr. Yunhe Zheng and Ms. Shiqi Liu for suggestions. The authors acknowledge the valuable comments from the referees. MW acknowledges that EELS data were acquired using the Nion UltraSTEM at the Cornell Center for Materials Research Shared Facilities which are supported through the NSF MRSEC program (DMR-1719875). MW acknowledges the kind assistance of Prof. David Muller and Mr. Malcolm (Mick) Thomas during these experiments. LB acknowledges the financial support of the Australian Research Council (DP150100558). The authors acknowledge funding from the Australian Research Council (LE110100223, LE0454166), for the Tecnai and Titan instrument respectively in MCEM.

Supplementary materials

Supplementary material associated with this article can be found, in the online version, at doi:10.1016/j.actamat.2020.116594.

References

[1] Y. Shimomura, Annealing of Secondary Defects in Quenched Aluminum, J. Phys. Soc. Jpn. 20 (6) (1965) 965–979.
[2] C. Cawthorne, E.J. Fulton, Voids in irradiated stainless steel, Nature 216 (1967) 575–576.
[3] J. Williams, J. Wong-Leung, Voids and Nanocavities in Silicon, Top. Appl. Phys. (2010) 113–146.
[4] M. Kiritani, S. Yoshida, A new type aggregation of quenched-in vacancies in aluminum, J. Phys. Soc. Jpn. 18 (6) (1963) 915.
[5] M. Kiritani, Formation of Voids and Dislocation Loops in Quenched Aluminum, J. Phys. Soc. Jpn. 19 (5) (1964) 618–631.
[6] L.M. Clarebrough, P. Humble, M.H. Loretto, Voids in Quenched Copper, Silver and Gold, Acta Metall 15 (6) (1967) 1007–1023.
[7] P.R. Okamoto, H. Wiedersich, Segregation of alloying elements to free surfaces during irradiation, J. Nucl. Mater. 53 (1974) 336–345.
[8] J.E. Epperson, R.W. Hendricks, K. Farrell, Studies of voids in Neutron-irradiated aluminum single crystals: 1. Small-angle X-ray scattering and transmission electron microscopy, Philos. Mag. 30 (4) (1974) 803–817.
[9] S.R. Nutt, A. Needleman, Void nucleation at fiber ends in Al-SiC composites, Scr. Metall. 21 (5) (1987) 705–710.
[10] M.E. Kassner, T.A. Hayes, Creep cavitation in metals, Int. J. Plasticity 19 (10) (2003) 1715–1748.
[11] L. Bourgeois, G. Bougaran, J.F. Nie, B.C. Muddle, Voids formed from solidifying tin particles in solid aluminium, Philos. Mag. Lett. 90 (11) (2010) 819–829.
[12] J.R. Black, Electromigration—A brief survey and some recent results, IEEE Trans. Electron Devices 16 (4) (1969) 338–347.
[13] H. Xu, C. Liu, V.V. Silberschmidt, S.S. Pramana, T.J. White, Z. Chen, V.L. Acoff, New mechanisms of void growth in Au–Al wire bonds: Volumetric shrinkage and intermetallic oxidation, Scr. Mater. 65 (7) (2011) 642–645.

[14] H. Jin, W.Y. Lu, J.W. Foulk, A. Mota, G. Johnson, J. Korellis, An Examination of Anisotropic Void Evolution in Aluminum Alloy 7075, Exp. Mech. 53 (9) (2013) 1583–1596.
[15] I.I. Balachov, E.N. Shcherbakov, A.V. Kozlov, I.A. Portnykh, F.A. Garner, Influence of radiation-induced voids and bubbles on physical properties of austenitic structural alloys, J. Nucl. Mater. 329-333 (2004) 617–620.
[16] P.G. Manusmare, H.P. Leighly, Void-strengthening in aluminum and its nature, Acta Metall 24 (11) (1976) 1047–1052.
[17] J.M.P. Alperin, Failure mechanisms and models for semiconductor devices, 2002.
[18] S. Coyle, M.C. Netti, J.J. Baumberg, M.A. Ghanem, P.R. Birkin, P.N. Bartlett, D.M. Whittaker, Confined Plasmons in Metallic Nanocavities, Phys. Rev. Lett. 87 (17) (2001) 176801.
[19] D.O. Sigle, E. Perkins, J.J. Baumberg, S. Mahajan, Reproducible Deep-UV SERRS on Aluminum Nanovoids, J. Phys. Chem. Lett. 4 (9) (2013) 1449–1452.
[20] Y. Zhu, P.N.H. Nakashima, A.M. Funston, L. Bourgeois, J. Etheridge, Topologically Enclosed Aluminum Voids as Plasmonic Nanostructures, ACS Nano 11 (11) (2017) 11383–11392.
[21] K.H. Westmacott, R.E. Smallman, P.S. Dobson, Annealing of voids in quenched aluminium and determination of surface energy, Met. Sci. J. 2 (1) (1968) 177–181.
[22] Z. Zhang, T. Liu, A.E. Smith, N.V. Medhekar, P.N.H. Nakashima, L. Bourgeois, Mechanisms of Void Shrinkage in Aluminium, J. Appl. Crystallogr. 49 (5) (2016) 1459–1470.
[23] K. Farrell, J. Bentley, D.N. Braski, Direct observation of radiation-induced coated cavities, Scr. Metall. 11 (3) (1977) 243–248.
[24] H. Hardy, The ageing characteristic of ternary aluminium copper alloys with cadmium, indium, or tin, J. Inst. Met. 80 (9) (1952) 483–492.
[25] L. Bourgeois, J.F. Nie, B.C. Muddle, On the Role of Tin in Promoting Nucleation of the θ' Phase in Al-Cu-Sn, Mater. Sci. Forum 396-402 (2002) 789–794.
[26] L. Bourgeois, C. Dwyer, M. Weyland, J.F. Nie, B.C. Muddle, The magic thicknesses of θ' precipitates in Sn-microalloyed Al–Cu, Acta Mater 60 (2) (2012) 633–644.
[27] J.M. Silcock, The effect of quenching on the formation of g.p. zones and θ' in al cu-alloys, The Philos. Mag. 4 (46) (1959) 1187–1194.
[28] P.A. Midgley, M. Weyland, 3D electron microscopy in the physical sciences: the development of Z-contrast and EFTEM tomography, Ultramicroscopy 96 (3) (2003) 413–431.
[29] P. Gilbert, Iterative methods for the three-dimensional reconstruction of an object from projections, J. Theor. Biol. 36 (1) (1972) 105–117.
[30] C.P. David, Visualization and analysis of crystal structures using CrystalMaker software, Z. Kristallogr. Cryst. Mater 230 (9-10) (2015) 559–572.
[31] A.P. Sutton, Interfaces in crystalline materials, Oxford, Clarendon, Oxford, 2006.
[32] R.E. Smallman, A.H.W. Ngan, Chapter 3-Physical Metallurgy and Advanced Materials Engineering, 7th Edition, OxfordButterworth- Heinemann, 2007.
[33] O. Melikhova, J. Kuriplach, J. Čížek, I. Procházka, Vacancy–solute complexes in aluminum, Appl. Surf. Sci. 252 (9) (2006) 3285–3289.
[34] S. Pogatscher, H. Antrekowitsch, M. Werinos, F. Moszner, S.S.A. Gerstl, M.F. Francis, W.A. Curtin, J.F. Löffler, P.J. Uggowitzer, Diffusion on Demand to Control Precipitation Aging: Application to Al-Mg-Si Alloys, Phys. Rev. Lett. 112 (22) (2014) 225701.
[35] L. Bourgeois, C. Dwyer, M. Weyland, J.-F. Nie, B.C. Muddle, Structure and energetics of the coherent interface between the θ' precipitate phase and aluminium in Al–Cu, Acta Mater 59 (18) (2011) 7043–7050.
[36] T.E. Volin, R.W. Balluffi, Annealing kinetics of voids and the Self-diffusion coefficient in aluminum, Phys. Status Solidi (b) 25 (1) (1968) 163–173.
[37] L. Bourgeois, T. Wong, X.Y. Xiong, J.F. Nie, B.C. Muddle, Interaction between Cu and Sn in the Early Stages of Ageing of Al-1.7at.%Cu-0.01at.%Sn, Mater. Sci. Forum 519-521 (2006) 495–500.
[38] S. Pogatscher, H. Antrekowitsch, H. Leitner, T. Ebner, P.J. Uggowitzer, Mechanisms controlling the artificial aging of Al–Mg–Si Alloys, Acta Mater 59 (9) (2011) 3352–3363.
[39] M. Griffiths, C.D. Cann, R.C. Styles, Neutron irradiation damage in 64% cold–worked Titanium, J. Nucl. Mater. 149 (2) (1987) 200–211.
[40] M. Griffiths, R.C. Styles, C.H. Woo, F. Phillipp, W. Frank, Study of point defect mobilities in zirconium during electron irradiation in a high-voltage electron microscope, J. Nucl. Mater. 208 (3) (1994) 324–334.
[41] W. Xu, Y. Zhang, G. Cheng, W. Jian, P.C. Millett, C.C. Koch, S.N. Mathaudhu, Y. Zhu, In-situ atomic-scale observation of irradiation-induced void formation, Nat. Commun. 4 (2013) 2288.
[42] M.J. Kelley, V. Ponec, Surface composition of alloys, Prog. Surf. Sci. 11 (3) (1981) 139–244.
[43] J. Liu, X. Zhang, M. Chen, L. Li, B. Zhu, J. Tang, S. Liu, DFT study on surface properties and dissolution trends of Al (1 0 0) surfaces doped with Zn, Ga, In, Sn and Pb, Appl. Surf. Sci. 257 (9) (2011) 4004–4009.
[44] G. Richter, K. Hillerich, D.S. Gianola, R. Mönig, O. Kraft, C.A. Volkert, Ultrahigh Strength Single Crystalline Nanowhiskers Grown by Physical Vapor Deposition, Nano Lett 9 (8) (2009) 3048–3052.
[45] Y. Qi, G. Richter, E. Suadiye, L. Klinger, E. Rabkin, Interdiffusion in bimetallic Au–Fe nanowhiskers controlled by interface mobility, Acta Mater 197 (2020) 137–145.
[46] L.D. Marks, L. Peng, Nanoparticle shape, thermodynamics and kinetics, J. Phys. Condens. Matter 28 (5) (2016) 053001.
[47] G. Wulff, XXV. Zur Frage der Geschwindigkeit des Wachsthums und der Auflösung der Krystallflächen, Z. Kristallogr. Cryst. Mater 34 (1) (1901) 449–530.
[48] S. Sivaramakrishnan, J. Wen, M.E. Scarpelli, B.J. Pierce, J.-M. Zuo, Equilibrium shapes and triple line energy of epitaxial gold nanocrystals supported on TiO2 (110), Phys. Rev. B 82 (19) (2010) 195421.
[49] L. Bourgeois, J.F. Nie, B.C. Muddle, Assisted nucleation of θ' phase in Al–Cu–Sn: the modified crystallography of tin precipitates, Philos. Mag. 85 (29) (2005) 3487–3509.
[50] B. Noble, Theta-prime precipitation in aluminium-copper-cadmium alloys, Acta Metall 16 (3) (1968) 393–401.
[51] H. Chen, Y. Yang, Z. Hu, K. Huo, Y. Ma, Y. Chen, X. Wang, Y. Lu, Synergism of C5N Six-Membered Ring and Vapor−Liquid−Solid Growth of CNx Nanotubes with Pyridine Precursor, J. Phys. Chem. B 110 (33) (2006) 16422–16427.